Reaction of NH (X) with Oxygen in a Solid Xenon Matrix: Formation and Infrared Spectrum of Imine Peroxide, HNOO

Sandra L. Laursen,*,† James E. Grace, Jr.,† Roger L. DeKock,‡ and Steven A. Spronk‡

Contribution from the Department of Chemistry, Kalamazoo College, Kalamazoo, Michigan 49006, and Department of Chemistry and Biochemistry, Calvin College, Grand Rapids, Michigan 49546

Received March 10, 1997. Revised Manuscript Received August 26, 1998

Abstract: The reaction between molecular oxygen and the imidogen radical NH in their ground electronic states has been investigated in solid cryogenic rare gas matrices. A photolabile product forms upon annealing a xenon matrix containing oxygen and trapped NH radicals produced by in situ UV photodissociation of hydrazoic acid. The product is identified as imine peroxide, HNOO, by its infrared spectrum and its photoisomerization to nitrous acid, with support from the calculated vibrational spectrum and ^{18}O isotope shifts. The reaction is essentially activationless. Some aspects of the potential energy surface for this species are delineated by the conditions under which HNOO is formed and destroyed. This is the first detection of this compound, a 1,3-dipole isoelectronic with ozone and peroxymethylene.

Introduction

The present study focuses on the reaction of ground-state NH ($X\ ^3\Sigma^-$) with molecular oxygen.

$$NH\ (X\ ^3\Sigma^-) + O_2\ (X\ ^3\Sigma_g^-) \rightarrow HNOO\ (X\ ^1A) \qquad (1)$$

The reaction is carried out by photolyzing HN_3 in a solid xenon matrix codoped with O_2. Ground-state NH ($X\ ^3\Sigma^-$) is trapped in the matrix upon relaxation of the initially formed excited NH radical. After annealing the matrix, infrared features ascribed to HNOO are observed.

Reactions of NH have been studied for their importance in combustion and astrophysical systems and are interesting as well in comparison with reactions of isoelectronic species O and CH_2.[1−7] Most studies of NH reactions have been performed on the lowest excited electronic state, NH ($a\ ^1\Delta$), because this state is very reactive and because it is easily and selectively prepared by photodissociation of HN_3 or HNCO. Direct dissociation of HN_3 into NH ($X\ ^3\Sigma^-$) + N_2 ($X\ ^1\Sigma_g^+$) or of HNCO into NH ($X\ ^3\Sigma^-$) + CO ($X\ ^1\Sigma^+$) is spin-forbidden on the ground electronic potential energy surface,[8,9] so the problem of preparing NH specifically in the ground triplet state has been solved instead through a variety of thermal, chemical, and photolytic schemes.[10−18] However, all these schemes necessarily lead to hot ground-state NH molecules in a distribution of energy states.

In our experiments, NH is formed initially in the first excited singlet state by photodissociation of HN_3 but relaxes to the triplet ground state by matrix quenching of the excited state. The time scale of the experiment is long, so that the trapped NH radicals are fully quenched to 12 K before the matrix is annealed to initiate diffusion and activationless reaction of ground-state NH. FTIR spectroscopy of the matrix-isolated products enables identification of product channels from both the initial photochemical reaction of excited NH and the thermal reaction of ground-state NH.

Gas-phase kinetic studies of the reaction of ground-state NH with oxygen have identified the major products as NO + OH but suggest that the reaction proceeds through one or more intermediates.[19,20] From NH and O_2, several structural isomers of HNO_2 are possible minima on the HNO_2 potential energy

* To whom correspondence should be addressed. Current address: National Oceanographic and Atmospheric Administration, R/E/AL2, 325 Broadway, Boulder, CO 80303.

† Kalamazoo College.

‡ Calvin College.

(1) Dean, A. M.; Chou, M.-S.; Stern, D. In *Chemistry of Combustion Processes*; A.C.S. Symp. Ser. 249; American Chemical Society: Washington, DC, 1984; Chapter 5, p 71.

(2) Blint, R. J.; Dasch, C. J. In *Chemistry of Combustion Processes*; A.C.S. Symp. Ser. 249; American Chemical Society: Washington, DC, 1984; Chapter 6, p 87.

(3) Perry, R. A.; Siebers, D. L. *Nature* **1986**, *324*, 657 and references therein.

(4) Kirby, K. P.; Goldfield, E. M. *J. Chem. Phys.* **1991**, *94*, 1271.

(5) Krasnopolsky, V. A.; et al. *Nature* **1986**, *321*, 269. Moreels, G.; et al. *Nature* **1986**, *321*, 271.

(6) Gustaffson, B. *Annu. Rev. Astron. Astrophys.* **1989**, *27*, 701 and references therein.

(7) Vetter, R.; Zülicke, L.; Koch, A.; van Dishoek, E. F.; Peyerimhoff, S. D. *J. Chem. Phys.* **1996**, *104*, 5558 and references therein.

(8) Baronavski, A. P.; Miller, R. G.; McDonald, J. R. *Chem. Phys.* **1978**, *30*, 119 and references therein.

(9) Drozdoski, W. S.; Baronavski, A. P.; McDonald, J. R. *Chem. Phys. Lett.* **1979**, *64*, 421.

(10) Brazier, C. R.; Ram, R. S.; Bernath, P. F. *J. Mol. Spectrosc.* **1986**, *120*, 381.

(11) Röhrig, M.; Wagner, H. Gg. *Ber. Bunsen-Ges. Phys. Chem.* **1994**, *98*, 858 and 864.

(12) Cox, J. W.; Nelson, H. H.; McDonald, J. R. *Chem. Phys.* **1985**, *96*, 175.

(13) Röhrig, M.; Wagner, H. Gg. *Ber. Bunsen-Ges. Phys. Chem.* **1994**, *98*, 1073.

(14) Hack, W.; Wagner, H. Gg.; Zasypkin, A. *Ber. Bunsen-Ges. Phys. Chem.* **1994**, *98*, 156.

(15) Stephenson, J. C.; Casassa, M. P.; King, D. S. *J. Chem. Phys.* **1988**, *89*, 1378.

(16) Kajimoto, O.; Yamamoto, T.; Fueno, T. *J. Phys. Chem.* **1979**, *83*, 429.

(17) Harrison, J. A.; Whyte, A. R.; Phillips, L. F. *Chem. Phys. Lett.* **1986**, *129*, 346.

(18) Quandt, R. W.; Hershberger, J. F. *J. Phys. Chem.* **1995**, *99*, 16939.

(19) Hack, W.; Kurtzke, H.; Wagner, H. Gg. *J. Chem. Soc., Faraday Trans. 2* **1985**, *81*, 949.

(20) Zetzsch, C.; Hansen, I. *Ber. Bunsen-Ges. Phys. Chem.* **1978**, *82*, 830.

10.1021/ja970749i CCC: $15.00
Published on Web 11/20/1998

surface, as shown below and as found in computational studies published by Melius and Binkley[21] and Fueno et al.[22]

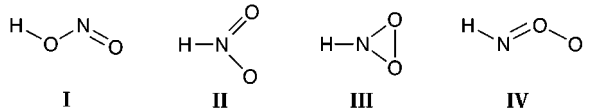

I **II** **III** **IV**

Both cis and trans isomers of nitrous acid (**I**) are well-known. A second structural isomer, HNO_2, hydrogen nitryl (**II**), has been identified recently.[23] The cyclic dioxaziridine (**III**) has not been observed. It is predicted to be stable, but insertion of NH into the OO bond requires an activation energy, and the barrier to further ring-opening to form **II** is low.[22] Rather, simple addition (reaction 1) of O_2 and NH in their ground electronic states should lead to isomer **IV**, imine peroxide.[22]

Both a simple valence-bond model and calculations[22,24−27] at a variety of levels of sophistication argue that, much like ozone, HNOO should have a singlet ground electronic state with substantial diradical character. The most important resonance structures are shown below.

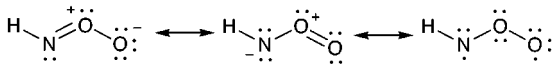

V **VI** **VII**

HNOO is a member of the class of molecules known as 1,3-dipoles, the electronic structure of which has been described in terms of the relative importance of the zwitterionic versus diradical structures.[28] In HNOO, the zwitterionic resonance structures **V** and, to a lesser extent, **VI** contribute to some degree, strengthening the NO and OO bonds beyond a single bond, but they are destabilized by the positive charge on the center oxygen, while all atoms have normal valence in the diradical structure **VII**. This is quite similar to the situation in ozone.

We report here the infrared detection, photochemical reaction, and computational modeling of imine peroxide, a novel intermediate formed in reaction 1. The paper is organized as follows: the methods and results of the matrix isolation experiments are presented, followed by the methods and results of the computational studies. The Discussion section first identifies the products formed at each stage: after initial photolysis; after annealing, including IR spectral assignments for the new intermediate; and after secondary photolysis. The dynamics of the experiments are interpreted, with key features of the potential energy surface for the HNOO system revealed by the conditions for forming and destroying the new species. Finally, the molecule is compared with the isoelectronic species ozone and peroxymethylene, and some general conclusions are drawn.

Experimental Methods

The experiments were performed at Kalamazoo College following standard matrix isolation techniques. Mixtures of hydrazoic acid (HN_3), oxygen, and rare gas were prepared in a glass vacuum line evacuated to a typical pressure of 1.5×10^{-5} Torr. An HN_3:O_2:Xe ratio near 0.7−1:5:550, determined manometrically, was used in most experiments. HN_3 was formed by heating sodium azide and octadecanoic acid to 90−100 °C. To minimize the explosion hazard, HN_3 pressure was kept below 5 Torr. Mixtures remained stable upon storage in glass bulbs for up to several months. The stated purity of O_2, Xe, and Ar was 99.9995% (Purity Gas Co.), 99.995% (AGA), and 99.999% (Purity Gas Co.), respectively, and these gases were used without further purification. Oxygen-18 was obtained from Isotec at 99 atom % purity. Mixed-isotope O_2 was obtained from Icon Services at 61 atom % ^{18}O.

Samples were deposited through needle valves at a rate of 0.5 to 1.0 mmol h^{-1} onto a CsI window held at 35.0 ± 0.4 K for Xe matrices and 18.0 ± 0.4 K for Ar matrices, using an APD Model HC-2 closed-cycle helium refrigerator and Scientific Instruments Model 9620-1 controller. For mixtures with HN_3:rare gas ratios near 1:500, typically 3−5 mmol of the gas mixture was deposited, so that IR absorptions for reactants were strong but the samples were still optically transparent to UV and visible photolysis. After deposition, the sample was cooled slowly to 12 K for spectroscopy and photolysis. The rotatable cold head was mounted in a shroud evacuated to $\leq 5 \times 10^{-6}$ Torr and equipped with CsI windows for IR spectroscopy and a fused silica (quartz) photolysis window.

FTIR spectra (100 scans) were collected with a Nicolet Magna-IR 550 spectrometer with DTGS detector in the range 400−4000 cm^{-1} at a resolution of 0.5 cm^{-1}. The beam path was purged with dry air from a Balston 75-52 FTIR purge gas generator.

Tunable narrow-band photolysis was done with a PTI illumination system based on a 200-W Hg/Xe lamp in a water-cooled A1010 housing. Photolysis wavelengths were selected by using a 0.25-m monochromator (PTI model 01−001) with a grating ruled at 600 lines mm^{-1} and slits set for a 20-nm bandwidth (fwhm). The first UV photolysis was at a wavelength of 254 nm. Annealed samples were heated to 50 K at about 1 K min^{-1}, then, after several minutes, cooled to 12 K at the same rate. A second series of photolyses was done at wavelengths from 800 to 300 nm.

Experimental Results

I. Photolysis and Annealing of $HN_3/O_2/Xe$ Matrices. Most experiments were performed in $HN_3/O_2/Xe$ matrices; experiments with varied composition or sample treatment are described in the next section. Mixtures of $HN_3/O_2/Xe$ 1:5:550 were photolyzed at 254 nm at 12 K. In all mixtures, the vibrational features of the parent HN_3 (IR-active fundamentals near 3298, 2133, 1263, 1144, and 535 cm^{-1})[29] disappeared rapidly, with essentially complete (≥95%) depletion in 2 h of photolysis. Figures 1 and 2 show the FTIR spectra of the initially deposited matrix (spectrum a) and of the matrix after UV photolysis at 254 nm (spectrum b). As seen in the figures, a number of new features appeared in the samples. By comparison with literature data and our own studies of HN_3/Xe and HN_3/H_2O/Xe, these were identified with known products. For clarity in presentation, they are identified here as *cis*- and *trans*-HONO, NH_2OH, N_2H_2, and NH; these assignments are supported in the Discussion section. Features assigned to NH_2OH and N_2H_2 were stable to further annealing and photolysis of the sample, while those assigned to HONO and NH continued to change, as described below. A complete table of observed FTIR frequencies and intensities and a summary of the intensity changes in these samples are available in the Supporting Information.

When samples of $HN_3/O_2/Xe$ 1:5:550 already photolyzed at 254 nm were annealed to 50 K and recooled to 12 K, several interesting changes were observed, as can be seen by comparing spectra b and c in Figures 1 and 2. The photoproduct features at 3132.2, 3120.5, and 3109.8 cm^{-1}, assigned to NH, disappear completely. An example of the changing intensity of the HONO bands is shown in Figure 3 and described in detail below. The

(21) Melius, C. F.; Binkley, J. S. In *The Chemistry of Combustion Processes*; ACS Symp. Ser. 249; Sloane, T. M., Ed.; American Chemical Society: Washington, DC, 1984; p 104.
(22) Fueno, T.; Yokoyama, K.; Takane, S.-y. *Theor. Chim. Acta* **1992**, *92*, 299−308.
(23) Koch, T. G.; Sodeau, J. R. *J. Phys. Chem.* **1995**, *99*, 10824.
(24) Hiberty, P. C.; Leforestier, C. *J. Am. Chem. Soc.* **1978**, *100*, 2012.
(25) Hiberty, P. C.; Ohanessian, G. *J. Am. Chem. Soc.* **1982**, *104*, 66.
(26) Yamaguchi, K. *J. Mol. Struct. (THEOCHEM)* **1983**, *103*, 101.
(27) Kahn, S. D.; Hehre, W. J.; Pople, J. A. *J. Am. Chem. Soc.* **1987**, *109*, 1871.
(28) See, for example: Huisgen, R. In *1,3-Dipolar Cycloaddition Chemistry*; Padwa, A., Ed.; Wiley: New York, 1984; Chapter 1, p 1.
(29) Shimanouchi, T. *J. Phys. Chem. Ref. Data* **1977**, *6*, 993.

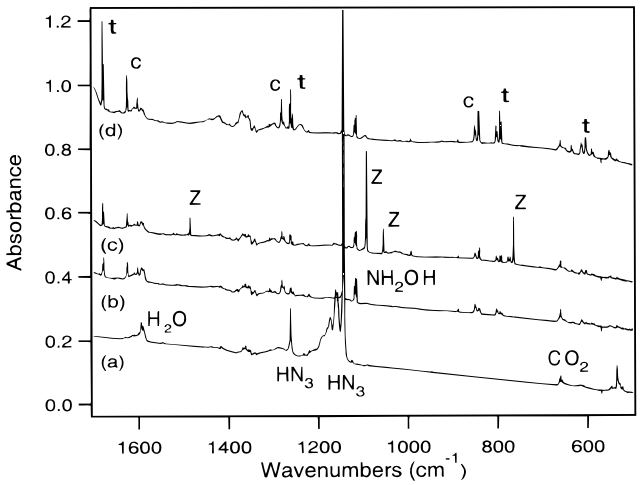

Figure 1. FTIR spectra of the $HN_3/O_2/Xe$ 1:5.3:540 matrix in the region 1700−500 cm^{-1}. All spectra recorded at 12 K. c = *cis*-HONO, t = *trans*-HONO. (a) Matrix at 12 K after deposition of 4.97 mmol $HN_3/O_2/Xe$ 1:5.3:540 at 35 K. (b) Matrix a after 2.0 h of photolysis at $\lambda = 254$ nm. (c) Matrix b after annealing to 50 K and recooling to 12 K. (d) Matrix c after complete depletion of Z via a series of visible and UV photolyses: 1.5 h at $\lambda = 700$ nm, 1.0 h at 650 nm, 4.0 h at $\lambda = 600$ nm, 1.0 h at $\lambda = 500$ nm, 1.0 h at $\lambda = 400$ nm, 10 min at $\lambda = 300$ nm.

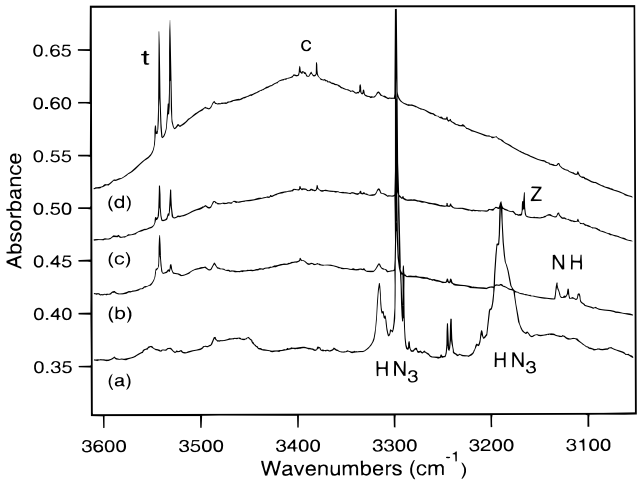

Figure 2. FTIR spectra of the $HN_3/O_2/Xe$ 1:5.3:540 matrix in the region 3600−3085 cm^{-1}. All spectra recorded at 12 K. Samples are the same as in Figure 1. c = *cis*-HONO, t = *trans*-HONO. (a) Matrix at 12 K after deposition of 4.97 mmol $HN_3/O_2/Xe$ 1:5.3:540 at 35 K. (b) Matrix a after 2.0 h of photolysis at $\lambda = 254$ nm. (c) Matrix b after annealing to 50 K and recooling to 12 K. (d) Matrix c after complete depletion of Z via a series of visible and UV photolyses: 1.5 h at $\lambda = 700$ nm, 1.0 h at $\lambda = 650$ nm, 4.0 h at $\lambda = 600$ nm, 1.0 h at $\lambda = 500$ nm, 1.0 h at $\lambda = 400$ nm, 10 min at $\lambda = 300$ nm.

most dramatic change is the appearance of five new, strong absorptions. The most intense of these is at 1092.3 cm^{-1} (matrix sideband at 1094.0 cm^{-1}), and new absorptions at 1054.5 (1048.9), 764.0 (771.9, 776.6), 1485.5, and a doublet at 3167.3/3165.5 cm^{-1} are also clearly identified. The new features begin to grow in immediately upon warming, with the stronger bands visible at temperatures as low as 20 K, increasing as the temperature is raised, and maximized near 50 K. Upon recooling to 12 K the vanished absorptions do not reappear, while the new features sharpen, and at 12 K, all five new features have the characteristic narrow bandwidths of a well-defined matrix-isolated species. The relative intensities of the strongest four bands at 1092.3, 1054.5, 764.0, and 1485.5 cm^{-1} are quite

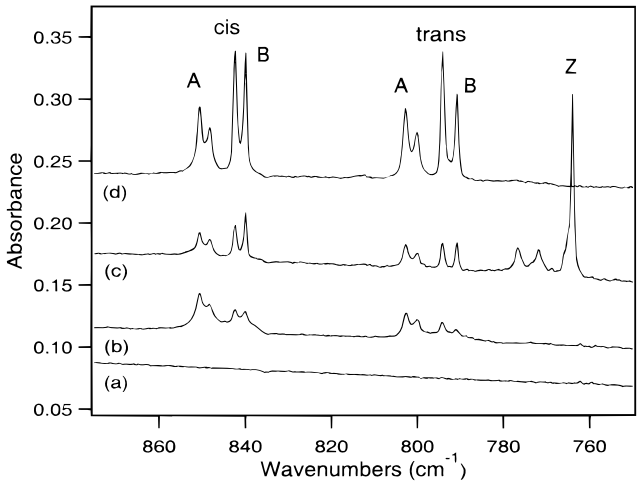

Figure 3. FTIR spectra of the $HN_3/O_2/Xe$ 1:5.3:540 matrix, expanded in the region 875−750 cm^{-1}. All spectra recorded at 12 K. Samples are the same as in Figures 1 and 2. c = *cis*-HONO, t = *trans*-HONO. (a) Matrix at 12 K after deposition of 4.97 mmol of $HN_3/O_2/Xe$ 1:5.3:540 at 35 K. (b) Matrix a after 2.0 h of photolysis at $\lambda = 254$ nm. (c) matrix b after annealing to 50 K and recooling to 12 K. (d) Matrix c after complete depletion of Z via a series of visible and UV photolyses: 1.5 h at $\lambda = 700$ nm, 1.0 h at $\lambda = 650$ nm, 4.0 h at $\lambda = 600$ nm, 1.0 h at $\lambda = 500$ nm, 1.0 h at $\lambda = 400$ nm, 10 min at $\lambda = 300$ nm.

constant; they are included in Table 1 (and 2). The 3167.3/3165.5 cm^{-1} feature is weak and its intensity is difficult to measure precisely, but its intensity qualitatively tracks the other four. We thus consider these five absorptions to characterize the same single product, referred to as product Z, which is formed in $HN_3/O_2/Xe$ matrices upon 254-nm irradiation followed by annealing.

Samples containing Z were next irradiated at long wavelengths with the Hg−Xe lamp and monochromator system. At wavelengths of 600, 500, 400, and 300 nm, the five absorption features of Z disappeared and other absorptions grew. Samples containing Z were also irradiated at $\lambda = 800$, 700, and 650 nm. Filters of plastic film were used to remove second-order light and ascertain that any secondary photolysis observed was due to visible, not UV, photolysis. The high sensitivity of hydrazoic acid to UV but not visible wavelengths was used to verify the filter's effectiveness. It was found that radiation at wavelengths from 300 to 600 nm caused Z to disappear, while wavelengths longer than 650 nm did not.

When secondary photolysis of Z did occur, the frequencies and relative intensities of the absorptions that grew in were independent of photolysis wavelength. However, the rate at which Z absorptions disappeared and new features grew was quite rapid at 300 nm compared with that at visible wavelengths (400−600 nm). Figure 4 compares the growth behavior of the strongest absorption of Z in a typical set of long-wavelength photolyses with that of some of the absorptions (assigned to HONO) growing in. Because this plot is not corrected for photolysis lamp intensity, it does not directly reflect true photolysis efficiencies for the photodepletion of Z, but it does show that 300-nm radiation is much more effective than visible wavelengths. The strongest of the spectral features that grew in intensity upon long-wavelength irradiation of Z are near 840, 791, 1625, and 1677 cm^{-1}. The Supporting Information lists these in more detail.

Finally, the HONO vibrational bands showed a distinct splitting pattern that correlated to different kinetic behavior of the subbands. A spectral region that clearly illustrates this

Table 1. Comparison of Computed Frequencies, Intensities, and $^{16}O/^{18}O$ Isotope Ratios for *trans*-HNOO with Experimental Results

	expt			CCSD(T)		BLYP			B3LYP			HF	
mode	ν	*A* rel	16/18 ratio	ν	16/18 ratio	ν	*I* abs (*I* rel)	16/18 ratio	ν	*I* abs (*I* rel)	16/18 ratio	ν	*I* abs (*I* rel)
NH str	3165.5	7		3379		3204	22.4 (103)		3349	5.9 (8)		3625	25.4 (32)
$HN^{16}O^{18}O$	3165.5		1.000	3379	1.000	3204	22.5	1.000	3349	5.9	1.000		
$HN^{18}O^{16}O$	3165.5		1.000	3379	1.000	3204	22.5	1.000	3349	5.9	1.000		
$HN^{18}O^{18}O$	3165.5		1.000	3379	1.000	3204	22.5	1.000	3349	5.9	1.000		
HNO bend	1485.5	12		1553		1508	0.7 (3)		1579	6.1 (8)		1712	11.9 (15)
$HN^{16}O^{18}O$	1484.0		1.001	1552	1.001	1507	1.0	1.001	1577	7.1	1.001		
$HN^{18}O^{16}O$	1474.6		1.007	1542	1.007	1498	1.9	1.007	1566	10.2	1.008		
$HN^{18}O^{18}O$	1473.4		1.008	1541	1.008	1497	2.2	1.007	1565	11.3	1.009		
NO str	1092.3	100		1193		1088	21.9 (100)		1260	75.1 (100)		1748	80.3 (100)
$HN^{16}O^{18}O$	1088.0		1.004	1187	1.005	1086	33.2	1.002	1260	75.3	1.000		
$HN^{18}O^{16}O$	1060.4		1.030	1157	1.031	1060	12.0	1.026	1225	63.6	1.029		
$HN^{18}O^{18}O$	1056.3		1.035	1151	1.029	1057	24.3	1.029	1225	65.3	1.028		
OO str	1054.5	25		1068		1026	147.4 (675)		1116	121.1 (161)		971	69.4 (86)
$HN^{16}O^{18}O$	1029.1		1.025	1042	1.025	998	129.7	1.027	1084	115.4	1.029		
$HN^{18}O^{16}O$	1034.8		1.019	1048	1.020	1000	147.2	1.026	1093	119.1	1.021		
$HN^{18}O^{18}O$	1007.9		1.046	1020	1.047	972	128.5	1.055	1060	111.8	1.052		
torsion	764.0	57		770	1.006	787	59.6 (273)	1.006	835	64.0 (85)	1.006	815	340.8 (425)
$HN^{16}O^{18}O$	762.3		1.002	768	1.002	785	60.5	1.002	833	65.0	1.002		
$HN^{18}O^{16}O$	761.3		1.004	767	1.004	783	60.8	1.004	832	65.3	1.004		
$HN^{18}O^{18}O$	759.6		1.006	765	1.006	782	61.6	1.006	830	66.3	1.006		
NOO bend	not obs.			670		643	1.7 (8)		685	2.6 (4)		716	9.3 (12)
$HN^{16}O^{18}O$				656	1.020	630	2.0	1.021	671	2.1	1.020		
$HN^{18}O^{16}O$				660	1.015	634	1.6	1.014	675	2.6	1.015		
$HN^{18}O^{18}O$				647	1.035	621	1.9	1.035	661	2.2	1.036		

[a] The top row in the section for each mode refers to the normal $^{16}O_2$ isotopomer. The 16/18 ratio as described in the text. *A* rel = relative absorbance, scaled so that the absorbance of the NO stretching mode (strongest observed band) = 100. *I* abs = absolute intensity in km mol^{-1}. *I* rel = relative intensity, scaled so that the intensity of the NO stretching mode (strongest observed band) = 100.

splitting and growth behavior is seen in Figure 3. Type "A" features (e.g. 850.8/848.7 and 802.7/800.3 cm^{-1}) grew substantially upon initial UV photolysis, diminished slightly or not at all upon annealing, and grew again upon continued visible photolysis. Type "B" features (e.g. 842.6/840.0 and 794.1/791.0 cm^{-1}) were barely visible after initial UV photolysis, grew noticeably upon annealing, and continued to grow with further photolysis. A- and B-type features were observed for both *cis*- and *trans*-HONO and were often further split themselves. The growth profiles of Figure 4 show the distinct growth patterns of the two types of features.

II. Variation of Sample Treatment and Composition. After detection of Z in $HN_3/O_2/Xe$ matrices, studies were undertaken to establish the sample composition and treatment necessary to produce Z. Product Z was never observed immediately after 254-nm photolysis of $HN_3/O_2/Xe$ but was detected after subsequent annealing of the same samples. Nor was Z observed when a matrix of $HN_3/O_2/Xe$ was annealed without irradiation at 254 nm, though Z was then produced by irradiating and reannealing the same sample. Thus neither photolysis nor annealing alone leads to formation of Z. Finally, Z did not reappear when a sample containing Z was photodepleted completely and then reannealed and/or rephotolyzed. All our experiments indicate that the specific sequence of 254-nm photolysis and annealing, in that order, is required to produce the species Z, and that continued photolysis irreversibly destroys it.

We also investigated the composition of the matrix necessary for formation of Z. The highest yields of Z were observed in matrices prepared from samples containing both hydrazoic acid and oxygen, typically $HN_3/O_2/Xe$ 1:5:550, when treated by UV photolysis and annealing as described. When HN_3 was omitted (i.e. O_2/Xe 1:100), no Z was formed. However, minor amounts of Z were sometimes detected in samples with HN_3 but without added O_2. Detailed study shows that formation of Z can occur when trace oxygen from air is present in the matrix, and that deliberate addition of air to the matrix gas mixture dramatically enhances the yield of Z. All studies confirmed that both HN_3 and O_2 are prerequisite for formation of Z.

Oxygen-18 labeling was undertaken to help identify the new species Z. Matrices of $HN_3/^{18}O_2/Xe$ 0.7:5:550 were treated as above by 254-nm photolysis, annealing, and visible photolysis. The resulting FTIR absorptions (see Supporting Information) are readily assigned by comparing both frequencies and growth behavior to samples with use of unlabeled oxygen. These bands appear under identical conditions and undergo the same growth behavior as their unlabeled counterparts. New absorptions appearing at 1055.0, 1007.9, 759.6, 1473.4, and 3165.5 cm^{-1} correspond to the absorptions of Z in the unlabeled product and are listed in Tables 1 and 2.

Matrices containing $HN_3/O_2/HN_3$ 0.8:5.5:550 with the mixed-isotope oxygen (37% $^{18}O_2$, 48% $^{18}O^{16}O$, 15% $^{16}O_2$) were also treated by 254-nm photolysis, annealing, and visible photolysis. The resulting FTIR absorptions include the bands observed in the $^{16}O_2$ and $^{18}O_2$ experiments as well as a number of new features. In particular, for each of the four strongest absorptions of Z, a total of four bands is observed; the 3165/3167 cm^{-1} band of Z is also observed. These are listed in Tables 1 and 2. Figure 5 compares the observed absorptions in the 1000−1100 cm^{-1} region to the bands observed in experiments with $^{16}O_2$ and $^{18}O_2$.

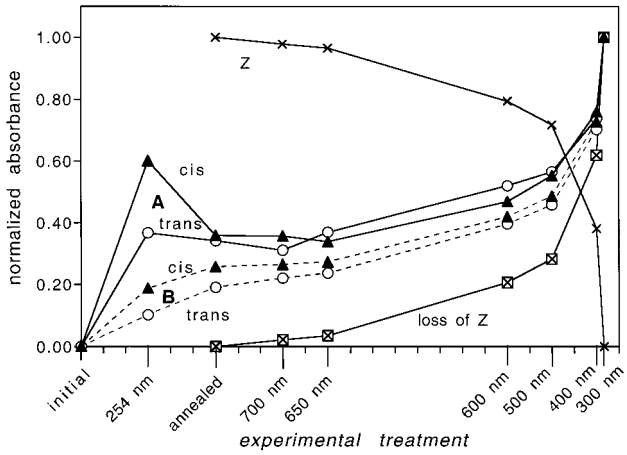

Figure 4. Growth profiles of product Z (HNOO) and HONO as a function of sample treatment. Horizontal axis indicates the sequential treatments in a single experiment on the same $HN_3/O_2/Xe$ 1:5.3:540 matrix as shown in Figures 1−3. The labeled points in the sequence are as follows: initial = as deposited; 254 nm = after 2.0 h of photolysis at $\lambda = 254$ nm; annealed = after annealing to 50 K; 700 nm = after 1.5 h of photolysis at $\lambda = 700$; 650 nm = after 1.0 h of photolysis at $\lambda = 650$ nm; 600 nm = after 4.0 h of photolysis at $\lambda = 600$ nm; 500 nm = after 1.0 h of photolysis at $\lambda = 500$ nm; 400 nm = after 1.0 h of photolysis at $\lambda = 400$ nm; 300 nm = after 10 min of photolysis at $\lambda = 300$ nm. Horizontal axis units are arbitrary from points "initial" to "annealed"; the axis is linear in time from points "annealed" to end, to indicate relative rates of photolysis. The text describes filters used in photolysis. All absorbances are measured as peak heights at 12 K and normalized to maximum absorbance. Curve Z (solid line, ×) shows absorbance of the Z band at 1092.3 cm^{-1}; "loss of Z" (solid line, boxed ×) shows relative depletion of absorbance at the 1092.3 cm^{-1} band (=1 − Z). For HONO absorptions, solid lines indicate HONO-A and dashed lines indicate HONO-B. Solid triangles indicate *cis*-HONO; open circles indicate *trans*-HONO. Absorbances plotted are the ν_4 N−O stretch of HONO: *cis*-A at 850.7 cm^{-1}; *cis*-B at 842.6 cm^{-1}; *trans*-A at 802.8 cm^{-1}; *trans*-B at 794.1 cm^{-1}.

Matrices of approximate composition 1:5:550 $HN_3/O_2/Xe$ appeared to optimize the yield of Z after annealing and reduce yields of bimolecular reaction products from initial HN_3 photolysis. More concentrated mixtures (e.g. $HN_3/O_2/Xe$ 1:10:100) led to a wide variety of products after initial 254-nm photolysis, mainly *cis*- and *trans*-HONO, but also NO, N_2O, O_3, and other species. Evidently oxygen radical chemistry becomes important in the concentrated samples.[30]

Finally, we looked for Z in Ar matrices. When samples containing $HN_3/O_2/Ar$ 1:4:500 were UV-photolyzed at 254 nm, photoproduct features appeared corresponding to those in Xe. Products at this point are the same as in Xe: *cis*- and *trans*-HONO, NH_2OH, and NH (at 3133.7 and 3140.2 cm^{-1}). Unlike Xe matrices, warming was not necessary: in samples allowed to stand at 12 K for several hours, new features appeared at 1096.6/1097.7 and 1058.0 cm^{-1}, matching two of the stronger features of Z in Xe, blue-shifted slightly by the Ar matrix. Upon annealing to 33−35 K, the NH features at 3133.7 and 3140.2 cm^{-1} disappeared partially, the 1097 and 1058 cm^{-1} features grew slightly more intense, and two more weak absorptions appeared at 776.3 and 1489.8 cm^{-1}, matching the next strongest absorptions of Z in Xe. All four features of Z were weak in comparison to their intensity in Xe and were not increased by further annealing, nor was NH fully depleted. The Z features were entirely photodepleted after a few minutes of photolysis at 300 nm.

To summarize the results, a new species Z is readily formed when a xenon matrix at 12 K containing both HN_3 and O_2 is first irradiated at 254 nm, then annealed to 50 K. New products grow in as Z is photodepleted by additional long-wavelength ($\lambda \leq 600$ nm) irradiation. Small quantities of Z can be created in solid Ar.

Computational Methods and Results

Computational studies were performed to model the geometries, relative energies, and vibrational spectra of the *cis*- and *trans*-HNOO isomers. Issues such as the barriers to cis−trans and HNOO−HONO isomerization, the nature of the excited states of HNOO, and the $HN-O_2$ binding energy, are being addressed in ongoing work and are not discussed here. We employed several theoretical methodologies: restricted Hartree−Fock (RHF), density functional theory (DFT) at several levels (LDFT, BLYP, and B3LYP),[31−34] and coupled cluster [CCSD(T)].[35,36] The 6-311G(d,p) basis set[37] used throughout all studies is of triple-ζ quality, with polarization functions on all atoms. DFT and RHF studies were done with Mulliken software;[38] the CCSD(T) work was performed with Gaussian 94.[39] Within Mulliken, the DFT methodology is implemented with the local correlation functional (LDFT) of Perdew and Wang.[40] All runs were done on an IBM RS/6000 workstation at Calvin College.

Stable conformers are obtained for imine peroxide at both cis and trans geometries. The cis isomer is calculated to be more stable by 12−21 kJ mol^{-1}, depending upon the theoretical method. Fueno and co-workers[22] completed a multireference calculation including configuration interaction (doubles), MRD-CI, at geometries found from a 6-electron, 6-orbital MCSCF calculation. In agreement with our result they found the cis isomer to be more stable by 18 kJ mol^{-1} at the MCSCF level, but the trans species was more stable by 3 kJ mol^{-1} at the MRD-CI level.

(30) Crowley, J. N.; Sodeau, J. R. *J. Phys. Chem.* **1989**, *93*, 4785.
(31) Lee, C.; Yang, W.; Parr, R. G. *Phys. Rev. B* **1988**, *37*, 785.
(32) Miehlich, B.; Savin, A.; Stoll, H.; Preuss, H. *Chem. Phys. Lett.* **1989**, *157*, 200.
(33) Becke, A. D. *Phys. Rev. A* **1988**, *38*, 3098.
(34) Becke, A. D. *J. Chem. Phys.* **1993**, *98*, 5648−5652.
(35) Purvis, G. D.; Bartlett, R. J. *J. Chem. Phys.* **1982**, *76*, 1910.
(36) Pople, J. A.; Head-Gordon, M.; Raghavachari, K. *J. Chem. Phys.* **1987**, *87*, 5968.
(37) Feller, D.; Davidson, E. R. *Reviews in Computational Chemistry*; Lipkowitz, K., Boyd, D. B., Eds.; VCH: New York, 1990; Vol. 1, pp 1−44.
(38) Lengsfield, B. H., III; Horn, H.; Swope, W. C.; Carter, J. T.; McLean, A. D.; Carter, J. T.; Replogle, E. S.; Rice, J. E.; Barnes, L. A.; Maluendes, S. A.; Lie, G. C.; Gutowski, M.; Rudge, W. E.; Sauer, S. P. A.; Lindh, R.; Andersson, K.; Chevalier, T. S.; Widmark, P.-O.; Bouzida, D.; Nesbet, R.; Singh, K.; Gillan, C. J.; Carnevali, P.; Liu, B.; Pacansky, J. *Mulliken*; 2.0 ed.; Lengsfield, B. H., III, Horn, H., Swope, W. C., Carter, J. T., McLean, A. D., Carter, J. T., Replogle, E. S., Rice, J. E., Barnes, L. A., Maluendes, S. A., Lie, G. C., Gutowski, M., Rudge, W. E., Sauer, S. P. A., Lindh, R., Andersson, K., Chevalier, T. S., Widmark, P.-O., Bouzida, D., Nesbet, R., Singh, K., Gillan, C. J., Carnevali, P., Liu, B., Pacansky, J., Eds.; IBM Research Division, Scientific & Technical Application Software, Almaden Research Center: San Jose, CA, 1996.
(39) Frisch, M. J.; Trucks, G. W.; Schlegel, H. B.; Gill, P. M. W.; Johnson, B. G.; Robb, M. A.; Cheeseman, J. R.; Keith, T. A.; Petersson, G. A.; Montgomery, J. A.; Raghavachari, K.; Al-Laham, M. A.; Zakrzewski, V. G.; Ortiz, J. V.; Foresman, J. B.; Cioslowski, J.; Stefanov, B. B.; Nanayakkara, A.; Challacombe, M.; Peng, C. Y.; Ayala, P. Y.; Chen, W.; Wong, M. W.; Andres, J. L.; Replogle, E. S.; Gomperts, R.; Martin, R. L.; Fox, D. J.; Binkley, J. S.; Defrees, D. J.; Baker, J.; Stewart, J. P.; Head-Gordon, M.; Gonzalez, C.; Pople, J. A. *Gaussian 94*, Revision D.1, D.3, and D.4 ed.; Frisch, M. J., Trucks, G. W., Schlegel, H. B., Gill, P. M. W., Johnson, B. G., Robb, M. A., Cheeseman, J. R., Keith, T. A., Petersson, G. A., Montgomery, J. A., Raghavachari, K., Al-Laham, M. A., Zakrzewski, V. G., Ortiz, J. V., Foresman, J. B., Cioslowski, J., Stefanov, B. B., Nanayakkara, A., Challacombe, M., Peng, C. Y., Ayala, P. Y., Chen, W., Wong, M. W., Andres, J. L., Replogle, E. S., Gomperts, R., Martin, R. L., Fox, D. J., Binkley, J. S., Defrees, D. J., Baker, J., Stewart, J. P., Head-Gordon, M., Gonzalez, C., Pople, J. A., Eds.: Pittsburgh, PA, 1995.
(40) Perdew, J. P.; Wang, Y. *Phys. Rev. B* **1992**, *45*, 1324.

Table 2. Comparison of Computed Frequencies, Intensities, and $^{16}O/^{18}O$ Isotope Ratios for *cis*-HNOO with Experimental Results

	expt			CCSD(T)		BLYP			B3LYP			HF	
mode	ν	*A* rel	16/18 ratio	ν	16/18 ratio	ν	*I* abs (*I* rel)	16/18 ratio	ν	*I* abs (*I* rel)	16/18 ratio	ν	*I* abs (*I* rel)
NH str	3165.5	7		3268		3092	33.3 (39)		3226	2.1 (2)		3498	14.8 (17)
$HN^{16}O^{18}O$	3165.5		1.000	3268	1.000	3092	33.3	1.000	3226	2.1	1.000		
$HN^{18}O^{16}O$	3165.5		1.000	3268	1.000	3092	33.3	1.000	3226	2.1	1.000		
$HN^{18}O^{18}O$	3165.5		1.000	3268	1.000	3092	33.3	1.000	3226	2.1	1.000		
HNO bend	1485.5	12		1502		1465	28.6 (34)		1529	42.5 (44)		1820	36.7 (43)
$HN^{16}O^{18}O$	1484.0		1.001	1502	1.000	1464	28.9	1.000	1528	42.7	1.000		
$HN^{18}O^{16}O$	1474.6		1.007	1493	1.006	1454	29.2	1.007	1518	45.2	1.008		
$HN^{18}O^{18}O$	1473.4		1.008	1493	1.006	1453	29.6	1.008	1517	45.4	1.008		
NO str	1092.3	100		1215		1126	84.7 (100)		1309	95.7 (100)		1683	86.0 (100)
$HN^{16}O^{18}O$	1088.0		1.004	1212	1.003	1125	91.3	1.001	1309	95.2	1.000		
$HN^{18}O^{16}O$	1060.4		1.030	1178	1.032	1100	68.5	1.023	1275	79.8	1.026		
$HN^{18}O^{18}O$	1056.3		1.035	1175	1.034	1099	76.3	1.024	1275	80.4	1.026		
OO str	1054.5	25		1062		979	120.0 (142)		1082	60.3 (63)		1072	90.7 (106)
$HN^{16}O^{18}O$	1029.1		1.025	1034	1.027	952	106.7	1.028	1050	55.4	1.030		
$HN^{18}O^{16}O$	1034.8		1.019	1039	1.022	951	123.7	1.029	1056	65.3	1.025		
$HN^{18}O^{18}O$	1007.9		1.046	1010	1.051	924	109.2	1.060	1023	59.3	1.057		
torsion	764.0	57		874		894	62.9 (74)		944	71.3 (74)		721	112.8 (130)
$HN^{16}O^{18}O$	762.3		1.002	872	1.002	892	62.7	1.002	942	71.1	1.002		
$HN^{18}O^{16}O$	761.3		1.004	869	1.006	888	63.3	1.006	939	71.8	1.005		
$HN^{18}O^{18}O$	759.6		1.006	867	1.008	887	63.1	1.008	936	71.5	1.008		
NOO bend		not obs.		656		620	15.1 (18)		662	17.7 (19)		674	8.2 (10)
$HN^{16}O^{18}O$				643	1.021	607	14.6	1.021	649	17.5	1.020		
$HN^{18}O^{16}O$				648	1.013	612	14.2	1.013	653	16.7	1.025		
$HN^{18}O^{18}O$				635	1.034	599	13.7	1.034	641	16.5	1.033		

[a] The top row in the section for each mode refers to the normal $^{16}O_2$ isotopomer. The 16/18 ratio as described in the text. *A* rel = relative absorbance, scaled so that the absorbance of the NO stretching mode (strongest observed band) = 100. *I* abs = absolute intensity in km mol^{-1}. *I* rel = relative intensity, scaled so that the intensity of the NO stretching mode (strongest observed band) = 100.

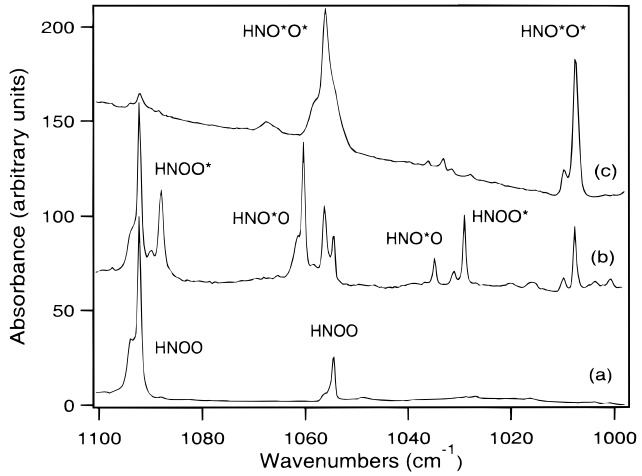

Figure 5. FTIR spectra of $HN_3/O_2/Xe$ matrices of varying oxygen isotope composition, expanded in the region 1100−1000 cm^{-1}. All spectra recorded at 12 K. (a) $HN_3/^{16}O_2/Xe$ 1:5:540 after 254-nm photolysis and annealing to 50 K. (b) HN_3/O_2 (61 atom % ^{18}O)/Xe 0.7:5:550 after 254-nm photolysis and annealing to 50 K. (c) $HN_3/^{18}O_2/Xe$ 0.8:5:550 after 254-nm photolysis and annealing to 50 K. O* designates the ^{18}O atom.

Bond lengths and bond angles at the two energy minima determined by RHF, BLYP, B3LYP, and CCSD(T) methods are summarized in Table 3. Tables 1 and 2 display the harmonic vibrational frequencies and intensities of *cis*- and *trans*-imine peroxide computed by these methods, for the four possible oxygen isotopomers. Intensities are not available for the CCSD-(T) frequencies.

Table 3. Geometries of *cis*- and *trans*-HNOO Calculated by Several Computational Methods

		CCSD(T)	BLYP	B3LYP	HF
		cis-HNOO			
distance (Å)	N−H	1.0404	1.0508	1.0406	1.0237
	N−O	1.2895	1.2893	1.2588	1.1800
	O−O	1.3063	1.3325	1.3025	1.3284
angle (deg)	H−N−O	103.46	104.30	104.86	106.53
	N−O−O	118.84	120.50	120.51	118.72
dihedral	H−N−O−O	0	0	0	0
		trans-HNOO			
distance (Å)	N−H	1.0315	1.0416	1.0304	1.0131
	N−O	1.3056	1.3120	1.2747	1.1908
	O−O	1.2928	1.3106	1.2851	1.2921
angle (deg)	H−N−O	99.39	99.31	100.70	104.58
	N−O−O	115.96	116.99	117.65	118.62
dihedral	H−N−O−O	180	180	180	180

An assessment of the reliability of these methods for a molecule like imine peroxide is in order. Like ozone, HNOO shows significant diradical character.[22,41] It is known that Hartree−Fock theory, which does not take electron correlation into account, is unable to describe adequately the geometry and vibrational frequencies of ozone and other species for which a single determinant description is inadequate.[42] Density functional theory provides results that are reasonably accurate, even for

(41) Takane, S.-y.; Fueno, T. *Theor. Chem. Acta* **1994**, *87*, 431−439.
(42) Bartlett, R. J.; Stanton, J. F. *Reviews in Computational Chemistry*; Lipkowitz, K., Boyd, D. B., Eds.; VCH: New York, 1994; Vol. 5, pp 65−169.
(43) Sander, W.; Schroeder, K.; Muthusamy, S.; Kirschfeld, A.; Kappert, W.; Boese, R.; Kraka, E.; Sosa, C.; Cremer, D. *J. Am. Chem. Soc.* **1997**, *119*, 7265−7270.
(44) Dixon, D. A.; DeKock, R. L. *J. Chem. Phys.* **1992**, *97*, 1157−1161.

molecules that require significant post-Hartree−Fock correlation treatments.[43] In fact, there are cases in which treatments such as CISD and CASSCF were still very poor, but DFT provided good results compared to experiment.[44]

CCSD(T) describes the geometry of many molecules very well, including the difficult cases of O_2H_2 and ozone.[45] It also is an excellent method for predicting harmonic vibrational frequencies for "well-behaved" molecules,[46] but still results in errors of up to 120 cm^{-1} for ozone.[42] It is noteworthy that CCSD(T) is still based upon a single reference electronic configuration as being a suitable approximation. Ozone, isoelectronic to HNOO, needs at a minimum a two-configuration wave function to properly describe its ground-state electronic structure.[47] The most recent theoretical work on ozone includes iterative triple excitation, CCSDT,[48] and CISD[TQ].[49] Both papers show that even at this level of treatment, there are deviations of roughly 30−50 cm^{-1} from the experimentally determined harmonic vibrational frequencies. Table 3 suggests that inclusion of correlation will be equally necessary for HNOO: the DFT and CCSD(T) structures differ substantially from the RHF geometries, which are nearly identical to those previously published.[50]

Discussion

I. Products Formed on Initial 254-nm Photolysis. The products of 254-nm photolysis of $HN_3/O_2/Xe$ 1:5:550 matrices are readily assigned by comparison with literature data. The strongest of these are due to the two isomers of nitrous acid, *cis*-HONO (3397.0, 1625.3, 850.8/848.7 cm^{-1}) and *trans*-HONO (3542.2, 1679.9/1677.5, 802.7/800.3, 613.5/603.4 cm^{-1}).[30,51−53] These bands also change intensities upon annealing and grow upon continued long-wavelength photolysis of product Z after annealing, as discussed in detail below. A multiplet near 1115 cm^{-1} matches well with the strongest vibrational band of hydroxylamine, with matrix splitting.[54] Diimide, N_2H_2, with bands at 3130.4, 1276.9/1275.2, and 1308.7/1306.0 cm^{-1}, was sometimes observed, particularly in more concentrated matrices.[55−58] The hydroxylamine and diimide features did not change upon later annealing and photolysis of the matrix.

Formation of HONO, NH_2OH, and N_2H_2 upon primary photolysis is straightforward to explain. UV excitation forms HN_3 ($^1A''$), a dissociative state that yields excited NH (a $^1\Delta$) and ground-state N_2,[8] and excited NH readily undergoes bimolecular reaction. In a matrix, NH (a $^1\Delta$) reacts with oxygen directly to form HONO,[59] the major product at this point. In the gas phase, HONO dissociates to OH and NO or NO_2 + H.[10,60,61] Singlet NH also reacts directly with water, an inevitable trace impurity, to form hydroxylamine,[62−64] as confirmed in our photolysis studies of $HN_3/H_2O/Xe$. Diimide may form from reaction of NH (a $^1\Delta$) with HN_3 or NH.[55,56] The fact that the absorptions of all three products are weak, despite the nearly complete consumption of HN_3, shows that the concentration of HN_3-reactant cage pairs of any type is relatively low.

The weak but distinct 3132.2-cm^{-1} absorption is assigned to NH based on comparison with literature spectra,[56,59] on our studies of HN_3/Xe matrices, and on its behavior upon annealing. From annealing and concentration studies this band could be distinguished from the NH stretch of N_2H_2. Two weaker bands at 3120.5 and 3109.8 cm^{-1} show the same behavior as the 3132.2-cm^{-1} band and are assigned to NH as well. Although NH rotates nearly freely in its ground electronic state,[65,66] the observed 11−12-cm^{-1} splittings do not reproduce the rotational structure and other splitting observed for NH in Xe matrices,[65−67] perhaps indicating that rotation is hindered by a nitrogen cage partner.[68] These bands are ascribed to trapping sites of NH in Xe and resemble lattice site splittings for NH in N_2[56,63] and predicted for NH in Ar.[69] No evidence is seen for differences in the depletion behavior of these sites upon annealing.

By referring to the NH seen in the spectrum after UV photolysis as "trapped NH", we emphasize that this molecule has escaped immediate reaction and is trapped in the matrix. It is not necessarily perfectly isolated and may be weakly complexed with the N_2 byproduct. Reactant concentrations are low enough in these samples that relaxation to the ground X ($^3\Sigma^-$) state may in fact be the major fate of the NH fragments. Bimolecular reaction products (N_2H_2, HONO, and NH_2OH) appear to account for a rather small fraction of the depleted HN_3. The infrared absorption of NH is notoriously feeble,[70] so even the weak absorption detected may reflect a rather substantial pool of unreacted NH trapped in the matrix. The NH bands are stable for hours or days at 12 K, and IR spectra are taken several minutes after photolysis has ended, at times quite long compared to the radiative lifetime of NH (a $^1\Delta$) in matrices.[68] Thus the NH detected in the IR spectrum represents a population of internally cold molecules in their ground (X $^3\Sigma^-$) electronic state.

II. Products Formed upon Annealing of UV-Irradiated Sample. The unknown product Z is identified by using several lines of evidence, beginning with the conditions in which Z is formed or not formed. Upon annealing, the vibrational band of trapped NH disappears, and the new set of Z absorptions appears. Clearly trapped NH reacts with something to form Z; the evidence shows that the second reactant is molecular oxygen. The appearance of five IR-active bands with correlated intensities shows that Z is a single polyatomic molecule. From the

(45) Helgaker, T.; Gauss, J.; Jørgenson, P.; Olsen, J. *J. Chem. Phys.* **1997**, *106*, 6430−6440.
(46) Thomas, J. R.; DeLeeuw, B. J.; Vacek, G.; Schaefer, H. F., III *J. Chem. Phys.* **1993**, *98*, 1336.
(47) Yamaguchi, Y.; Frisch, M. J.; Lee, T. J.; Schaefer, H. F., III; Binkley, J. S. *Theor. Chim. Acta* **1986**, *69*, 337−352.
(48) Watts, J. D.; Bartlett, R. J. *J. Chem. Phys.* **1998**, *108*, 2511−2514.
(49) Leininger, M. L.; Schaefer, H. F. *J. Chem. Phys.* **1997**, *107*, 9059−9062.
(50) Nakamura, S.; Takahashi, M.; Okazaki, R.; Morokuma, K. *J. Am. Chem. Soc.* **1987**, *109*, 4142.
(51) Jacox, M. E. *J. Phys. Chem. Ref. Data* **1990**, *19*, 1387 and references therein.
(52) Hall, R. T.; Pimentel, G. C. *J. Chem. Phys.* **1963**, *38*, 1889.
(53) Mielke, Z.; Tokhadze, K. G.; Latajka, Z.; Ratajczak, E. *J. Phys. Chem.* **1996**, *100*, 539.
(54) Withnall, R.; Andrews, L. *J. Phys. Chem.* **1988**, *92*, 2155.
(55) van Thiel, M.; Pimentel, G. C. *J. Chem. Phys.* **1960**, *32*, 133.
(56) Rosengren, K.; Pimentel, G. C. *J. Chem. Phys.* **1965**, *43*, 507.
(57) Craig, N. C.; Levin, I. W. *J. Chem. Phys.* **1979**, *71*, 400.
(58) Jensen, H. J. Aa.; Jørgensen, P.; Helgaker, T. *J. Am. Chem. Soc.* **1987**, *109*, 2895.
(59) Baldeschwieler, J. D.; Pimentel, G. C. *J. Chem. Phys.* **1960**, *33*, 1008.
(60) McDonald, J. R.; Miller, R. G.; Baronavski, A. P. *Chem. Phys.* **1978**, *30*, 133.
(61) Meaburn, G. M.; Gordon, S. *J. Phys. Chem.* **1968**, *72*, 1592.
(62) Kawai, J.; Tsunashima, S.; Sato, S. *Chem. Lett.* **1983**, 823.
(63) Milligan, D. E.; Jacox, M. E. *J. Chem. Phys.* **1964**, *41*, 2838.
(64) Sudhakar, P. V.; Lammertsma, K. *J. Am. Chem. Soc.* **1991**, *113*, 5219.
(65) McCarty, M., Jr.; Robinson, G. W. *J. Am. Chem. Soc.* **1959**, *81*, 4472.
(66) Bondybey, V. E.; Brus, L. E. *J. Chem. Phys.* **1975**, *63*, 794.
(67) Blindauer, C.; van Riesenbeck, N.; Seranski, K.; Winter, M.; Becker, A. C.; Schurath, U. *Chem. Phys.* **1991**, *150*, 93.
(68) Ramsthaler-Sommer, A.; Eberhardt, K. E.; Schurath, U. *J. Chem. Phys.* **1986**, *85*, 3760.
(69) Jansen, G.; Hess, B. A.; Marian, C. M.; Ángyán, J. G. *J. Phys. Chem.* **1993**, *97*, 10011.
(70) Chackerian, C., Jr.; Guelachvili, G.; López-Piñeiro, A.; Tipping, R. H. *J. Chem. Phys.* **1989**, *90*, 641.

fact that Z yields are highest when the matrix is relatively dilute, when oxygen-radical chemistry is also minimized, termolecular or higher clusters are not required for formation of Z. Of the possible products on the NH + O_2 surface, the HONO (**I**) and HNO_2 (**II**) isomers have known IR spectra and can be ruled out. The atom-transfer or recombination products, NO + OH, HNO (+O), and NO_2 (+H), also have known IR spectra that do not match the Z absorptions, nor is evidence of secondary O-atom or H-atom reactions seen. As shall be argued here, both chemical and spectroscopic evidence identify the new species Z as imine peroxide, HNOO.

Infrared Spectroscopic Assignments. The geometry of imine peroxide is expected to be planar but nonlinear, like HONO, with 6 IR-active vibrational modes (5 A′ + 1 A″). Infrared group frequencies for the nitroso oxide (NOO) group itself have not been reported, but the infrared spectrum of imine peroxide is readily assigned. The evidence used to make these assignments includes comparison with computed ab initio and DFT frequencies, ^{18}O isotope shifts, and comparison with the known vibrational spectra of ozone, nitrous acid, and other structurally related molecules.

Comparison of the data shown in Tables 1 and 2 shows generally good agreement between observed and calculated frequencies, intensities, and isotope shifts for the computational methods expected to be most reliable for this molecule. The RHF calculations are known to yield poor predictions for molecules such as imine peroxide. The tables illustrate this point and the RHF results are not discussed further. For both *cis*- and *trans*-HNOO, the BLYP, B3LYP, and CCSD(T) calculations predict an NH stretch near 3200 cm^{-1}, an HNO bend near 1500 cm^{-1}, NO and OO stretches near 1000−1200 cm^{-1} with the NO stretch higher in frequency, an out-of-plane mode in the 800−900-cm^{-1} region, and a low-intensity heavy-atom bend near 650 cm^{-1}. Calculated (BLYP and B3LYP) intensities predict that the strongest absorptions should be the NO and OO stretches and the out-of-plane mode, in agreement with our assignments; the B3LYP intensities are generally in better agreement with the observed intensities. Taking into account the fact that the calculated values are harmonic frequencies, unlike the observed frequencies, the calculations are in excellent agreement with the observations and provide strong support for the spectroscopic identification of this molecule as HNOO. A mode-by-mode examination of the assignments follows.

The strong Z absorptions at 1092.3 and 1054.5 cm^{-1} are assigned to the NO and OO stretches of imine peroxide. The splitting of both modes into four bands upon partial ^{18}O labeling (Figure 5) demonstrates definitively that the molecule contains two inequivalent O atoms, and the magnitude of the isotope shifts indicates that both modes involve substantial motion of the O atoms. Calculations on both HNOO and O_3 suggest that the NOO bonding in HNOO is quite similar to the OOO bonding in ozone,[24,27] and the observed frequencies are remarkably close to the ozone stretching frequencies at 1103 and 1042 cm^{-1} (gas phase).[29] It may be reasonable to think of HNOO as an "isotopically substituted" ozone molecule, since the NH group is of similar mass to an oxygen atom and is poorly coupled to the lower-frequency stretches. The isotope shifts are substantial for both modes, suggesting that the two stretching modes are strongly coupled. Isotope shift data in Tables 1 and 2 are presented as the ratio ν_{16}/ν_{18}, where ν_{16} designates the molecule with two ^{16}O atoms and ν_{18} designates a molecule with one or two ^{18}O atoms as noted. The observed $^{18}O_2$ isotope shift ratios of 1.035 (at 1092 cm^{-1}) and 1.046 (at 1054 cm^{-1}) compare well with the values for the stretching modes of ozone labeled the same way ($^{16}O^{18}O^{18}O$), 1.048 (at 1103 cm^{-1}) and 1.040 (at 1042 cm^{-1}).[71] In contrast, if the stretches are modeled as uncoupled Hooke's law oscillators, the predicted (harmonic) isotope ratio is 1.061 for the $^{18}O^{18}O$ stretch and 1.028 for the $N^{18}O$ stretch. The pattern of isotope shift upon single and double ^{18}O substitution shows that the 1054-cm^{-1} band involves substantial motion of both O atoms, while the 1092-cm^{-1} band involves mainly motion of one O atom. We thus describe the 1054-cm^{-1} band as primarily OO stretch and the intense 1092-cm^{-1} band as primarily NO stretch.

For both *cis*- and *trans*-HNOO the calculations yield two intense bands centered in the 1000−1200-cm^{-1} region. In general the lower frequency of the two is close to both observed bands (1092 and 1054 cm^{-1}), while the upper frequency is above them, in one instance by more than 200 cm^{-1}. In all cases, the calculated splitting $\nu_{NO} - \nu_{OO}$ in the stretching frequencies is greater than the 38-cm^{-1} observed splitting. Bartlett and Stanton have discussed the challenges of computing stretching frequencies for ozone,[42] and similar difficulties may apply here. Still, all three computational methods predict a smaller difference $\nu_{NO} - \nu_{OO}$ for the trans (62 to 144 cm^{-1}) than for the cis isomer (147 to 227 cm^{-1}). Thus in this portion of the spectrum, the agreement between observed and calculated frequencies is better for *trans*-HNOO.

All three theoretical methods also predict that the $^{18}O_2$ isotope shift ratios of the two stretches will differ more from each other than is seen. For example, the CCSD(T) method predicts ratios of 1.047 and 1.029 for *trans*-HNOO, while the observed ratios are 1.045 and 1.036. However, in each case the predicted shift ratios are closer together for *trans*-HNOO than for *cis*-HNOO, and in general the isotope data for the sequentially ^{18}O-labeled compound better match the calculated shift ratios for *trans*-HNOO. The CCSD(T) method gives the best prediction of the isotope shift ratios.

Both ozone and imine peroxide are described as incorporating "two bonds midway between normal single and double linkages",[27] and comparison with other molecules supports this portrayal. The NO stretch at 1092.3 cm^{-1} is well below the nitro group frequencies in such molecules as NO_2 (1618, 1318 cm^{-1}),[29] CH_3NO_2 (1583, 1397 cm^{-1}),[72] and HNO_2 (1600, 1376 cm^{-1}),[23] as well as lower than the N═O stretch in HNO (1565 cm^{-1}).[73] However, the observed frequency is above that for an NO single bond, as in hydroxylamine, at 895 cm^{-1} in Ar,[54] or in oximes, e.g. $H_2C{=}N{-}OH$ at 893 cm^{-1}.[51] Further insight is gained by comparison with HONO, the bonding of which is well described by structure **I** above. In *trans*-HONO in Xe the NO stretching frequencies fall at 1680 and 794 cm^{-1}; the equivalent modes in *cis*-HONO absorb at 1626 and 842 cm^{-1} in Xe. The NO stretch of HNOO at 1092 cm^{-1} falls squarely between the N−O and N═O stretches of HONO, nearer the low-frequency end, as would be predicted from simple Lewis models.

The OO stretching absorption at 1054.5 cm^{-1} is near the OO stretches of ozone at 1103 and 1042 cm^{-1}.[29] This is not surprising considering that calculated OO bond lengths of HNOO are quite close to those calculated for ozone by the same method.[24,27] The 1054.5-cm^{-1} frequency is similar to OO stretches in molecules with peroxy groups, to which nitroso oxides have been compared.[74] The single OO bonds in HOOH

(71) Schriver-Mazzuoli, L.; De Saxce, A.; Lugez, C.; Camy-Peyret, C. *J. Chem. Phys.* **1995**, *102*, 690.
(72) Gorse, D.; Cavagnat, D.; Pesquer, M.; LaPouge, C. *J. Phys. Chem.* **1993**, *97*, 4262.
(73) Mélen, F.; Herman, M. *J. Phys. Chem. Ref. Data* **1992**, *21*, 831.
(74) Brinen, J. S.; Singh, B. *J. Am. Chem. Soc.* **1971**, *93*, 6623.

(877 cm^{-1})[29] and HOONO (952/957 cm^{-1} in Ar)[75] have stretching frequencies below that of HNOO, while higher-frequency OO stretches in radicals such as HO_2 (1101 cm^{-1} in Ar) and C_2H_5OO (1112 cm^{-1}) involve more double-bond character.[51]

The doublet at 3167.3/3165.5 cm^{-1} is assigned to the NH stretch. The lack of an ^{18}O isotope shift and the similarity to NH itself (3132.2 cm^{-1}) are consistent with the predicted weak binding of the NH and O_2 moieties.[22] The NH group is relatively little perturbed by formation of the NO bond, in contrast with the NH vibration of HNO_2 (**II**) at 3289 cm^{-1}.[70] The experimental values agree well with the calculated frequency and low intensity of this mode for both *cis*- and *trans*-HNOO.

The band at 1485.5 cm^{-1} is assigned to the HNO bend, close to the bending frequency of HNO (1505 cm^{-1} in Ar)[73] and above the less stiff HOO bends in HO_2 (1389 cm^{-1} in Ar)[51] and HOONO (1364/1373 in Ar)[75] and the HON bend in $HONH_2$ at 1351 cm^{-1}.[54] The proximity of the bending modes of HNOO and HNO is notable in light of Fueno's description of HNOO as a "zwitterionic O-oxide of hydrogen nitrosyl HNO".[22] Most of the modest ^{18}O isotope shift occurs upon labeling the central O atom, consistent with computed isotope shift ratios. The observed frequency and medium intensity are in good agreement with the calculations for both isomers, in all methods.

The absorption at 764.0 cm^{-1} is assigned to the out-of-plane bend, in agreement with the frequency and high intensity predicted for this mode. The small ^{18}O isotope shifts are consistent with a motion involving mainly the H atom. In all three methods a higher torsional frequency, by over 100 cm^{-1}, is predicted for the cis isomer, but the observed frequency agrees better with the lower predicted value for *trans*-HNOO. In addition, under all three methods the observed ^{18}O isotope shift ratios agree better with the predicted shift ratios for *trans*-HNOO than for *cis*-HNOO.

The calculations also predict a heavy-atom in-plane bend in the 600−700-cm^{-1} region. This vibration is comparable to the OOO bends in ozone (701 cm^{-1}),[29] the ONO bend of HNO_2 (792 cm^{-1} in Ar),[23] and the ONO bend in HOONO (773/783 in Ar).[75] No such absorption was detected in these experiments, consistent with the prediction of very low IR intensity for this vibration within all computational methods. In all methods, the calculated ^{18}O isotope shift ratios agree favorably with the observed isotope shifts for equivalently labeled ozone.[71]

These arguments show that the observed spectrum is in good agreement with the calculated vibrational modes. However, the calculations identify two stable isomers of HNOO, which should be easily distinguishable here given the narrow IR bandwidths of matrix samples. Tables 1 and 2 show that corresponding vibrational modes of *cis*- and *trans*-HNOO typically differ by 50−100 cm^{-1}. The much smaller (2−3 cm^{-1}) splittings that are seen in several of the bands of Z are instead characteristic of matrix site splittings. Thus the spectrum of Z appears to be that of a single isomer. Its absorptions plausibly match the calculations for either *cis*- or *trans*-HNOO, especially considering that the difference between experimental and calculated frequencies is of similar magnitude to the errors for similar molecules such as ozone.[42] We have already noted the most significant differences between the predicted spectra of *cis*- and *trans*-HNOO, namely in the frequencies and isotope shifts of the torsion, NO, and OO stretching modes. On the strength of these differences, reinforced by the recurrence of these patterns in all three computational methods, we conclude that the matrix FTIR spectrum best identifies the observed isomer as *trans*-HNOO.

III. Products Formed upon Visible Photolysis of Z. As Z is photodepleted upon longer-wavelength visible or UV photolysis, *cis*-HONO and *trans*-HONO grow in. The kinetic profiles (Figure 4) have the same shape and wavelength dependence, within experimental error, for the loss of Z and growth of HONO. This is further evidence that product Z is HNOO, since HNOO should isomerize readily to the more stable isomer HONO with a low activation energy.[21,22] In the gas phase, HONO generally fragments to OH + NO.[19,61] We detect a hint of this process via the appearance of a weak absorption at 1867.4 cm^{-1} corresponding to NO in a matrix.[30,59] Nitrous acid is formed here with less internal energy than in the gas-phase studies and is rapidly cooled in the solid, the matrix cage preventing extensive fragmentation.

The spectra (Figure 3) and growth behavior of the type A and B sets of bands suggest that they are due to two cage isomers of HONO. Type B features agree very well with the spectrum of HONO in Xe matrix, while type A features match those observed for HONO in Xe matrices lightly doped with N_2.[76] We thus assign HONO-A to a nitrogen complex, denoted HONO·N_2, and HONO-B to nitrous acid without perturbation from a nitrogen cage partner. Complexes of HONO with N_2 have been previously observed in Ar matrix and described computationally.[77] The growth behavior (Figure 4) supports these assignments. The major primary photoproduct (HONO-A) is HONO·N_2, formed upon direct UV excitation of HN_3 in an O_2-containing matrix. The N_2 cage partner is still present in close association with the HONO product until, upon annealing, some cages rearrange to stabilize an unperturbed HONO (B) product. Either the HONO·N_2 complex is not particularly strong or an even stronger complex is formed with the more polarizable xenon. Continued long-wavelength photolysis destroys imine peroxide and yields more of both cage isomers of HONO, in the same proportions in which they are present at the end of the annealing step, suggesting that this distribution is governed by the relative thermodynamic stability of the two cage complexes. Evidence of similar complexation does not appear in the HNOO spectrum. Ab initio calculations for HONO·N_2 predict that N_2 is hydrogen bonded to HONO through the OH group.[77] The less polar NH group in HNOO may not stabilize an N_2 complex.

The smaller splittings within each doublet, typically 2−3 cm^{-1}, are due to a different type of matrix effect. Since the relative intensities within the doublets remain constant throughout all the annealing and photolysis processes, and since the splittings are quite comparable for all isomers, these sites must represent stable or rapidly equilibrated matrix sites that form independently of whether the molecule is cis or trans, N_2-complexed or not. The splittings are quite similar to those observed for directly deposited HONO monomers in Ar.[53] A full explanation of these spectral splittings cannot be offered, but a modeling approach may provide insight.[67,78−80]

The cis/trans ratio of HONO does not change throughout the experiment, as seen in the fact that the growth profiles for both isomers have the same shape. Both the initial 254-nm photolysis

(75) Cheng, B.-M.; Lee, J.-W.; Lee, Y.-P. *J. Phys. Chem.* **1991**, *95*, 2814.

(76) Mielke, Z.; Tokhadze, K. G.; Talik, T. Manuscript in preparation.

(77) Mielke, Z.; Latajka, Z.; Kolodziej, J.; Tokhadze, K. G. *J. Phys. Chem.* **1996**, *100*, 11610.

(78) Winter, M.; Seranski, K.; Schurath, U. *Chem. Phys.* **1992**, *159*, 235.

(79) Agrawal, P. M.; Thompson, D. L.; Raff, L. M. *J. Chem. Phys.* **1994**, *101*, 9937.

(80) Raff, L. M. *J. Chem. Phys.* **1990**, 93, 3160.

beam and the $\lambda \leq 600$ nm light used in secondary photolysis provide more than enough energy to overcome the barrier to this isomerization (39 ± 1 kJ mol^{-1}),[81] so a thermally equilibrated population of HONO isomers is formed and maintained throughout these processes.

IV. Potential Energy Surface of HNOO. Several key features of the ground potential energy surface of HNOO are revealed by the conditions in which this compound is formed and destroyed. Inferences can also be made about the electronic excited states of HNOO from the observed photochemical activity of this compound.

Matrix Dependence of Formation of HNOO; Barrier to NH + O_2 Reaction. Imine peroxide is formed upon warming a matrix containing trapped NH and O_2. In xenon, it begins to form at 20 K and yields increase up to 50 K, while in argon, HNOO begins to form at 12 K and increase up to 33 K. Calculations predict that the gas-phase reaction of NH and O_2 should be activationless,[21,22] but in the solid state, warming is necessary to soften the matrix slightly and enable NH to escape its cage. Apkarian's group has shown that fluorine and oxygen atoms diffuse quite long distances in Kr and Xe matrices in this temperature range;[82,83] NH is small and should be similarly mobile. Benderskii and Wight have studied the isoelectronic reaction, geminate recombination of O (^{3}P) + O_2.[84,85] They found a low activation energy (2.0 ± 0.5 kJ mol^{-1}) to cage escape of ground-state O atoms in solid Xe, and an even lower value (0.38 ± 0.08 kJ mol^{-1}) in solid Ar. Since NH is nearly a free rotor in solid matrices, some HNOO may form simply by reorientation of NH toward an O_2 neighbor, such as in Ar where HNOO forms upon standing at 12 K. In general, however, we interpret the observed matrix dependence of the temperature at which HNOO forms to mean that diffusion of NH is the rate-limiting step. The barrier to reaction is then characteristic of the solid matrix and not a barrier on the isolated NH + O_2 potential energy surface. This is consistent with the prediction of an activationless reaction in the gas phase.

An interesting difference in the two matrices is that in Xe, all the reactant NH is consumed and a high HNOO yield results, while in Ar much of the NH remains after annealing, limiting the HNOO yield. In Ar NH may be permanently trapped in a distinct site. Differences in crystallinity, defect frequency, or cage size in the two matrices may affect diffusion.[84] Greater NH absorbance relative to HONO suggests that the quantum yield of trapped NH from 254-nm photolysis is higher in Xe. Increased spin−orbit coupling in the heavy-atom matrix may enhance intersystem crossing of the initially formed NH (a $^1\Delta$), making relaxation to the ground state competitive with chemical reaction. A pronounced matrix heavy-atom effect on branching ratios has been observed for the reaction of NH with dimethylacetylene[86] and other photoreactions in matrices.[87−89]

Finally, relative IR intensities of imine peroxide from the thermal NH (X $^3\Sigma^-$) + O_2 reaction and of nitrous acid from the photochemical NH (a $^1\Delta$) + O_2 reaction appear to suggest that rather more HNOO is formed than HONO. This may appear to contradict gas-phase reports that NH (a $^1\Delta$) is more reactive than NH (X $^3\Sigma^-$).[10,90] However, the inhomogeneity of the solid matrix must be taken into account. When excited HN_3 molecules dissociate, the NH (a $^1\Delta$) formed is both highly chemically reactive and only slowly physically quenched, even in a matrix.[68] Thus, NH (a $^1\Delta$) fragments with an O_2 nearest neighbor are likely to react and form HONO, while those escaping reaction long enough to relax to the ground electronic state will tend to be without a close oxygen neighbor. To react, these must diffuse through the matrix to encounter an O_2 reactant. Assuming a statistical distribution of precursors in a cubic close-packed lattice,[91] at these concentrations (1:5:550) fewer than 10% of the HN_3 molecules will have an O_2 neighbor in the first solvation shell, while over 30% will have at least one oxygen neighbor within the next, larger, solvation shell. If diffusion lengths for NH are similar to the 20−300-Å distances seen for fluorine and oxygen atoms,[82−84] the majority of NH molecules should encounter an O_2 during annealing. Thus high yields of imine peroxide in the thermal reaction are consistent with the proposed mechanism for its formation, while low yields of the photochemical product HONO are consistent with the small number of $HN_3 \cdot O_2$ precursor pairs trapped upon deposition of these matrices.

Ground-State Isomerism and Thermochemistry of HNOO. Though both cis and trans forms of imine peroxide should be stable, only one isomer is observed in the matrix, most likely the trans isomer. Thermochemical considerations may explain this observation. Both our own calculations and those of Fueno and co-workers find ground-state energies of *cis*- and *trans*-HNOO to be within a few kJ mol^{-1}, though which isomer is predicted to be more stable is quite sensitive to the computational method used.

If both isomers are formed initially but isomerization occurs before cooling to 12 K, an equilibrium distribution of isomers will be observed. At the low temperatures of these experiments, even a small difference in the stability of the two isomers can result in a large population difference. For instance, Fueno's value of 3 kJ mol^{-1} for the energy difference between HNOO isomers leads to a trans/cis ratio of over 1300:1 at 50 K. If comparable IR absorptivities for *cis*- and *trans*-HNOO vibrations are assumed (as supported by computed intensities), the strongest absorption of the less stable isomer will still be undetectable in our samples. In fact, a conservative estimate of the signal-to-noise ratio in our most intense HNOO spectrum yields a lower limit for the energy difference of 2 kJ mol^{-1}. Moreover, the calculations refer to isolated (gas-phase) molecules, while the experiments detect molecules solvated by a polarizable xenon matrix. The DFT calculations yield a dipole moment substantially larger for *trans*-HNOO (2.6 D) than for *cis*-HNOO (1.5 D), suggesting that xenon should preferentially stabilize the trans isomer. Alternately, trapping of a single isomer may be a result of reaction dynamics, for instance a small barrier (perhaps matrix-related) to form one isomer or a large barrier to rotational isomerization.

One clue to the thermodynamic stability of imine peroxide is the fact that it is not seen after UV photolysis, where it might be produced by reaction of hot NH (X $^3\Sigma^-$) after intersystem crossing of the initially formed NH (a $^1\Delta$). As argued above, NH (a $^1\Delta$) is so reactive that there may be rather few NH−O_2 pairs in which NH has relaxed to the ground state but is still close enough to O_2 to react. More importantly, NH (X) formed after intersystem crossing still has up to 151 kJ mol^{-1} of energy above the vibrationless level. Since no HNOO is trapped at this

(81) Shirk, A. E.; Shirk, J. S. *Chem. Phys. Lett.* **1983**, *97*, 549.
(82) Feld, J.; Kunttu, H.; Apkarian, V. A. *J. Chem. Phys.* **1990**, *93*, 1009.
(83) Danilychev, A. V.; Apkarian, V. A. *J. Chem. Phys.* **1993**, *99*, 8617.
(84) Benderskii, A. V.; Wight, C. A. *J. Chem. Phys.* **1996**, *104*, 85.
(85) Benderskii, A. V.; Wight, C. A. *J. Chem. Phys.* **1994**, *101*, 292.
(86) Collins, S. T.; Pimentel, G. C. *J. Phys. Chem.* **1984**, *88*, 4258.
(87) Laursen, S. L.; Pimentel, G. C. *J. Phys. Chem.* **1989**, *93*, 2328.
(88) Laursen, S. L.; Pimentel, G. C. *J. Phys. Chem.* **1990**, *94*, 8175.
(89) Singmaster, K. A.; Pimentel, G. C. *J. Mol. Struct.* **1989**, *194*, 215.
(90) Hack, W.; Wilms, A. *J. Phys. Chem.* **1989**, *93*, 3540 and references therein.
(91) Hallam, H. E., Ed. *Vibrational Spectroscopy of Trapped Species*; John Wiley: London, 1973.

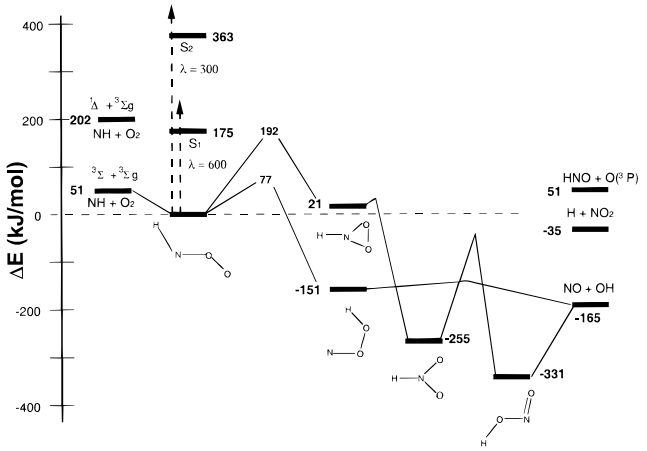

Figure 6. Potential energy profile for the NH + O_2 system. Energy levels are based on MRD-CI calculations with 6-31G** basis, by Fueno et al., ref 22. The values differ from the figure in that paper by the calculated difference in relative energies of *cis*- and *trans*-HNOO, 3 kJ mol^{-1}.

stage, this energy plus the exothermicity of the NH (X) + O_2 → HNOO reaction 1 itself must leave the nascent hot HNOO molecule above the barrier to further isomerization or fragmentation on the ground potential energy surface. Conversely, since HNOO is readily trapped when internally *cold* NH reacts with O_2, the barrier to further reaction must be greater than the energy released by reaction 1 alone, when the internal energy of the hot NH has already been dissipated to the matrix.

The NH (a→X) energy of 151 kJ mol^{-1} is well established,[10,90] but estimates of the exothermicity of reaction 1 vary from 27 to near 100 kJ mol^{-1}.[21,22] The barrier to isomerization of HNOO, which may be as low as 74 kJ mol^{-1},[22] puts an upper limit on the NH−O_2 binding energy. For the sake of comparison, the O (^{3}P) + O_2 exothermicity of 106.3 kJ mol^{-1} is well-characterized.[92]

Isomerization of HNOO to HONO. Ab initio calculations on this reaction predict two possible isomerization routes for HNOO on the ground electronic surface, as seen in the energy-level diagram in Figure 6.[21,22] Melius and Binkley studied the pathway involving ring closure of HNOO to form the cyclic isomer **III**, followed by OO bond breakage to give symmetric HNO_2 (**II**). Hydrogen nitryl then isomerizes to nitrous acid (**I**), the direct precursor to gas-phase products NO + OH. Fueno and co-workers confirm this route, calculating a total barrier of 189 kJ mol^{-1}, and offer an additional pathway involving 1,3-hydrogen migration to give HOON, which then decomposes to NO + OH, with a total activation energy of 74 kJ mol^{-1}. Confined in the matrix, the fragments likely combine to give HONO. Thus formation of HONO as the final product in the matrix is not taken to indicate the rearrangement route, especially since neither HNO_2 nor HOON intermediates are detected.

Thermal probing of the contours of the ground-state potential energy surface would destroy the matrix, but some information about the PES is obtained from the photochemical reaction that takes place. Because photochemical isomerization to HONO occurs at 600 nm but not at 650 nm, the threshold for photoisomerization can be placed between 188 and 201 kJ mol^{-1}. From this finding we can infer that the barrier to isomerization is no higher than 201 kJ mol^{-1}, and that the molecule must have an absorbing electronic state in this energy region. The onset of photoisomerization, which corresponds to a vertical excitation energy, is in good agreement with the (adiabatic) energy of the lowest excited singlet state predicted by Fueno, 175 kJ mol^{-1} for *trans*-HNOO or 188 kJ mol^{-1} for *cis*-HNOO. After excitation, isomerization may take place on the singlet excited surface or after internal conversion to a hot ground-state molecule. The hot ground-state molecule is born with enough energy to surpass the barrier to rearrangement on the ground PES, and any HOON or open or cyclic HNO_2 intermediate will rapidly rearrange before it can be detected. Ample thermal energy is available to equilibrate the final product HONO to yield the observed mixture of isomers.

The enhanced photodepletion of HNOO at $\lambda = 300$ nm relative to longer wavelengths evidently marks the opening of a new, very efficient photoreaction channel. This suggests that HNOO has a second, stronger absorption in the UV, in good agreement with theoretical predictions of a second excited singlet state at 363 kJ mol^{-1} for *trans*-HNOO or 402 kJ mol^{-1} for *cis*-HNOO, near the photon energy at $\lambda = 300$ nm (399 kJ mol^{-1}). With sufficient energy to overcome any isomerization barriers, imine peroxide is efficiently converted to the most stable product, HONO.

V. Comparison with Isoelectronic Species. Experimentally little is known of the nitroso oxides, of which HNOO is the simplest member, but they have long been of theoretical interest, like the other 1,3-dipoles.[28] Our experiments suggest that HNOO has properties much like its isoelectronic counterparts, ozone and peroxymethylene.

The analogy with ozone is especially close, as highlighted by the similar IR stretching frequencies. NH ($X\ ^3\Sigma^-$), like O (^{3}P) and CH_2 ($\tilde{X}\ ^3B_1$), reacts exothermically with ground-state O_2 ($X\ ^3\Sigma_g^-$). As in ozone formation,[92] there is essentially no barrier to the reaction of NH with oxygen. This contrasts with the apparent barrier (4−6 kJ mol^{-1}) to reaction of $^3CH_2 + O_2$.[93] The fact that HNOO is successfully stabilized in a matrix indicates that the exothermicity of the ^{3}NH + O_2 reaction is less than the ground-state barrier to further rearrangement or fragmentation, if the reactants are initially cold. This coupled with the theoretical predictions suggests that this reaction is more like the $^3O + O_2$ reaction ($\Delta H = -106.3$ kJ mol^{-1}) than the $^3CH_2 + O_2$ reaction ($\Delta H \approx -250$ kJ mol^{-1}).[94] The large exothermicity of reaction apparently leads to rearrangment or fragmentation of CH_2OO, since that adduct has not been detected despite much effort. The observations are consistent with the expectation that CH_2OO has less diradical character than imine peroxide and ozone.

The photochemical behavior and, by inference, the electronic absorption spectrum of HNOO agree strikingly with the spectral properties of ozone and the carbonyl oxides. The UV absorption cross section of ozone near 300 nm is nearly 3 orders of magnitude greater than that near 600 nm.[95] Several substituted analogues of peroxymethylene feature a strong absorption in the 300−400 nm region; these compounds are also quite photolabile at rather longer wavelengths, revealing a weaker, lower-energy absorption.[96−98] Both the experimental observa-

(92) Steinfeld, J. I.; Adler-Golden, S. M.; Gallagher, J. W. *J. Phys. Chem. Ref. Data* **1987**, *16*, 911 and references therein.

(93) Alvarez, R. A.; Moore, C. B. *J. Phys. Chem.* **1994**, *98*, 174.

(94) Kafafi, R. I.; Martinez, R. I.; Herron, J. T. *Molecular Structure and Energetics—Unconventional Chemical Bonding*; Liebman, J. F., Greenberg, A., Eds.; VCH: New York, 1988; Vol. 6, p 283. Cited in: Anglada, J. M.; Bofill, J. M.; Olivella, S.; Solé, A. *J. Am. Chem. Soc.* **1996**, *118*, 4636.

(95) Brasseur, G.; Solomon, S. *Aeronomy of the Middle Atmosphere*, 2nd ed.; D. Reidel: Dordrecht, 1986.

(96) Sander, W. W. *J. Org. Chem.* **1989**, *57*, 333 and references therein.

(97) Scaiano, J. C.; McGimpsey, W. G.; Casal, H. L. *J. Org. Chem.* **1989**, *54*, 1612 and references therein.

(98) Ganzer, G. A.; Sheridan, R. S.; Liu, M. T. H. *J. Am. Chem. Soc.* **1986**, *108*, 1517.

tions and theoretical predictions of the relative stability of the HNO_2 isomers and potential energy surface for rearrangement of HNOO strongly resemble the analogous chemistry for peroxymethylene.[93,99]

Conclusions

We have identified a new species, imine peroxide, formed in the ground-state reaction of NH and O_2 in cryogenic rare gas matrices. The activation energy for the reaction is very small and is associated with diffusion of NH in the matrix. The infrared spectrum of HNOO is in good agreement with the predictions of high-level coupled-cluster and density functional theory calculations. Its electronic structure resembles that of ozone, based on similarities in infrared and electronic absorptions. The molecule is photochemically active, isomerizing to nitrous acid upon irradiation with visible or UV light. Some clues about the shape of the ground-state potential energy surface for this molecule are provided by the energy dependence of this process. The observations are in good agreement with present and prior theoretical predictions about this molecule and are comparable with the isoelectronic species ozone and peroxymethylene.

The use of xenon as the matrix material enhances formation of HNOO. The heavy-atom matrix likely enhances intersystem crossing of NH (a $^1\Delta$) to NH (X $^3\Sigma^-$), so that the yield of trapped NH in the matrix is greater and more is available to react with O_2. Imidogen radicals may also be more mobile in Xe. The xenon matrix can be warmed to a higher temperature than can argon, and the larger cage size may facilitate diffusion. Although the rare gas matrix is inert in a chemical sense, it does help form and stabilize this novel intermediate and indicates the special role a solid environment can play in the chemistry of free radicals.

The method used here to study the reaction of NH with O_2 involves trapping the reactants separately in the matrix, then warming to induce reaction. Studies of the solid-state reaction chemistry of free radicals are important in designing schemes for forming and trapping free radicals in energetic solids for use as propellants. For the broader goal of identifying transient reaction intermediates by matrix isolation, this method is not a generally useful one. It will be effective only for reactions with very small activation energies, where these modest energies can be supplied thermally without destroying the matrix. However, those reactions include a group often difficult to study by other means, reactions between two open-shell species. Since free radical reactants are typically produced hot, by thermal or photochemical dissociation of a stable precursor, primary adducts typically disintegrate before they can be studied. Thus this very gentle method of inducing reaction within a cryogenic matrix should apply to other reactions between open-shell molecules. Future studies will focus on extending this method to reactions of NH and its analogues with other open-shell molecules to identify interesting intermediates.

Acknowledgment. A number of Kalamazoo College undergraduates made substantial contributions to this project by constructing the apparatus and performing related experiments. S.L.L. and J.E.G. thank Luke Chadwick, Stew Collins, Jamie Elsila, Becky Olson, Craig Ortsey, Jenny-Meade Pfennig, Hannah Ruggles, John Taylor, and Mike Thompson. Tom Massura and Forrest Duddles gave valuable technical assistance and Jeff Bartz helped with figure preparation. Zofia Mielke is thanked for sharing data on HONO complexes. Financial support was provided by a William and Flora Hewlett Award from the Research Corporation, by the donors of the Petroleum Research Fund, administered by the American Chemical Society, by the National Science Foundation under Grant No. CHE-9309827, and by Kalamazoo College. R.L.D.K. and S.A.S. wish to thank the Petroleum Research Fund, the Camille and Henry Dreyfus Foundation, and Calvin College for their support of the computational studies.

Supporting Information Available: A table including all FTIR frequencies and intensities for HN_3/O_2/Xe 1:5.3:540 and frequencies for $HN_3/^{18}O_2$/Xe 0.7:5:550 (4 pages, print/PDF). See any current masthead page for ordering information and Web access instructions.

JA970749I

(99) Wadt, W. R.; Goddard, W. A., III *J. Am. Chem. Soc.* **1975**, *97*, 3004.